Defence Science Journal, Vol. 59, No. 3, May 2009, pp. 230-238

REVIEW PAPER

Buckling Analysis of Composite Hexagonal Lattice Cylindrical Shell using Smeared Stiffener Model

M. Buragohain[1] and R. Velmurugan[2]

[1]*Advanced Systems Laboratory, Hyderabad–500058*
[2]*Indian Institute of Technology Madras, Chennai–600036*

ABSTRACT

Hexagonal lattice pattern formed by helical and circumferential ribs is the most common among different possible lattice patterns. An energy-based smeared stiffener model (SSM) is developed to obtain equivalent stiffness coefficients of a composite lattice cylindrical shell with such hexagonal lattice patterns. Using the equivalent stiffness coefficients, Ritz buckling analysis was carried out. Extensive finite element modelling covering different representative sizes have been carried out. SSM is validated by comparing the estimated buckling loads. Variation of material properties of rib unidirectional composites from those of normal unidirectional composites is accounted for in the energy formulations.

Keywords: Buckling analysis, smeared stiffener model, SSM, lattice patterns, Ritz buckling analysis

NOMENCLATURE

A_{ij}, B_{ij}, D_{ij}	Elements of stiffness matrices $\mathbf{A}, \mathbf{B}, \mathbf{D}$
$A^*_{ij}, B^*_{ij}, D^*_{ij}$	Elements of compliance matrices $\mathbf{A}^*, \mathbf{B}^*, \mathbf{D}^*$
b, h	Cross-sectional width and depth of stiffening ribs
D, L, R	Diameter, length, and radius (at mid-plane), respectively of the shell/lattice cylinder
e	Distance between the centreline and load (applied eccentrically)
$E_1, E_2, G_{12}, \nu_{12}$	2-D orthotropic material properties
h_k	z coordinate of the k^{th} ply
m, n	Half-wave numbers
M_x, M_y, M_{xy}	In-plane moment resultants
N_h	Number of pairs of helical ribs
$\mathbf{N}, \mathbf{M}$	Vectors of in-plane force and moment resultants
N_x, N_y, N_{xy}	In-plane force resultants
P_x, P_y, T_x	Axial compressive force, lateral compressive force and torque respectively
$\overline{\mathbf{Q}}$	Reduced transformed stiffness matrix of the composite laminate making the ribs
u, v, w	Displacements at a point (x, y, z) in the x, y, z directions, respectively
u_0, v_0, w_0	Displacements at a point in the mid-plane
U, V, Π	Strain energy, work done by external forces, and total potential energy respectively of the shell
U_{mn}, V_{mn}, W_{mn}	Amplitudes of generalised displacements
$U_{P_x}, U_{P_y}, U_{T_x}$	Strain energies under P_x, P_y, T_x, respectively
x, y, z	Axial, circumferential and radial coordinates as per cylindrical coordinate system
$\varepsilon_x, \varepsilon_y, \gamma_{xy}$	In-plane normal and shear strains
$\varepsilon_z, \gamma_{xz}, \gamma_{yz}$	Out-of-plane normal and shear strains
$\varepsilon^0_x, \varepsilon^0_y, \gamma^0_{xy}$	In-plane normal and shear strains in the mid-plane
$\varepsilon^1_x, \varepsilon^1_y, \gamma^1_{xy}$	Changes in curvatures in the mid-plane
$\boldsymbol{\varepsilon}^0, \boldsymbol{\varepsilon}^1$	Vectors of in-plane strains and changes in curvatures, respectively
$\sigma_x, \sigma_y, \sigma_z$	Normal stresses at a point
Δ	Surface area
$\tau_{xy}, \tau_{yz}, \gamma_{xz}$	Shear stresses at a point
θ	Angle of orientation of helical ribs wrt meridian

Subscripts

equ	Equivalent shell
rib	Rib segments
hco	Helical-to-helical crossovers
cco	Circumferential-to-helical crossovers

1. INTRODUCTION

Cylindrical shells are used in many weight-sensitive aerospace and other high-end applications. Buckling behaviour of such a structure under axial compression is of critical importance and grid-stiffened composite shells, on account of their very high specific strength and stiffness properties, provide an attractive alternative to traditional monolithic

Received 13 May 2008

metallic/composite shells. A special class of such structures is a lattice structure that comprises a grid of stiffening ribs without any skin. The stiffening ribs are basically unidirectional composites made by filament winding and these form an efficient system of load-bearing elements. Different lattice patterns such as diamond lattice with helical ribs only, hexagonal lattice with helical and circumferential ribs, and hexagonal lattice with helical and meridional ribs, etc can be designed. Out of the various lattice patterns, hexagonal pattern with helical and circumferential ribs is the most common and the study of buckling analysis of lattice composite cylindrical shell with such hexagonal lattice patterns has been presented.

There is a growing interest in grid-stiffened composite shells for their high-buckling resistance capabilities; but the subject is of relatively recent origin and open literature is somewhat limited. Three basic methods are used in the buckling analysis of a stiffened shell. These are:

(i) smeared stiffener model,
(ii) discrete model, and
(iii) branched plate and shell model.

Smeared stiffener approach is efficient in global buckling analysis and it is based on mathematical models that smear the stiffening ribs into an equivalent ply. Several authors[1-8] have adopted the smearing approach in buckling analysis of stiffened shells. A general note on the development of grid-stiffened composite shells, covering design and analysis procedure as well as issues on manufacturing and testing, is given by Vasiliev[1], *et al.*. Initial design/analysis is based on a continuum model where stiffening ribs are smeared, based on rib spacing, to arrive at an equivalent shell. Jones[2] also used rib spacing in relation to rib cross-sectional width as the criterion to smear the ribs. Velmurugan[3], *et al*. have presented a quick and efficient method useful for parametric studies in the initial design phase of a grid-stiffened shell. Wodesenbet[4], *et al.* and Kidane[5], *et al* have presented a global buckling analysis model wherein smeared stiffener approach is used through force/moment analysis of a unit cell to determine stiffness contribution of the stiffeners. Transverse strain and shear strains are neglected.

An improved smeared stiffener model that accounts for transverse shear flexibility, is used by Jaunky[6,7], *et al.* and Damodar[8], *et al.* In this model, skin-stiffener interaction effects are included by considering a neutral surface profile of the skin-stiffener combination. Smearing criterion is based on equivalence of strain energies and involves considering the strain energies of the skin and stiffeners using strain compatibility equations. Slinchenko[9], *et al.* used the smearing approach, on the basis of rib spacing, to determine structural stiffness matrix for finite element analysis of grid-stiffened structure.

The discrete approach and branched plate/shell approach are computationally more involved and these methods are normally used in the final design phase of a grid-stiffened shell. Several authors have worked in these directions, e.g. Huybrechts[10], *et al.* and Wang[11].

Issues involved in buckling analysis of composite structures are complex and the subject is still evolving as is evident from a large number of publications that are appearing regularly. For example, Jaunky[12], *et al*. have presented a discussion of shell theories as applied to buckling of cylindrical laminated composite shell. Similarly, some simple solutions for buckling behavior of cylindrical shell are presented by Geier[13], *et al.*

Filament-wound composite grid-stiffened shells throw up numerous possible design configurations in terms of various design elements. Once decided to use a particular lattice pattern (such as hexagonal pattern with helical and circumferential ribs), the choice of design elements comes down; but still the designer needs to consider many possible configurations that involve factors like number of ribs, cross-sectional details, spacing of ribs, rib orientation, etc. As a result, in the initial design phase, wherein broad choice of design elements is made, finite element analysis (FEA) is time-consuming and also it is more economical to use a quick tool, such as smeared stiffener model to find global buckling load.

While several smeared stiffener models are available in the open literature that account for material property variation, from the crossover zone to the unidirectional rib segment is rare. The aim of this study is to evolove a simple and efficient analytical model, which takes this material property variation into account, for global buckling analysis that would be useful in the initial design phase. This model is intended to be used for narrowing down design choices involving many possible configurations, so that in the final design phase, finite element analysis with finer and local details can be carried out effectively. A cylindrical composite shell made up of a grid of continuous ribs has been considered. Smearing the ribs into an equivalent shell is done by equating the strain energy of the stiffened shell to that of the equivalent shell and the methodology involved use of simplified force distribution in the formulation of strain energy. Ritz buckling analysis of the equivalent composite shell is carried out to find out the critical buckling load.

2. ANALYTICAL FORMULATION

2.1 Kinematic Relations

Classical laminated shell theory[14] (CLST) is based on the following displacement field

$$\begin{Bmatrix} u(x,y,z) \\ v(x,y,z) \\ w(x,y,z) \end{Bmatrix} = \begin{Bmatrix} u_0(x,y) - z\dfrac{\partial w_0}{\partial x} \\ v_0(x,y) - z\dfrac{\partial w_0}{\partial y} \\ w_0(x,y) \end{Bmatrix} \quad (1)$$

Displacements and the coordinate directions are defined in Fig. 1. Following Kirchhoff hypothesis, $\varepsilon_z = \gamma_{xz} = \gamma_{yz} = 0$ and the strain-displacement relations for CLST are given by:

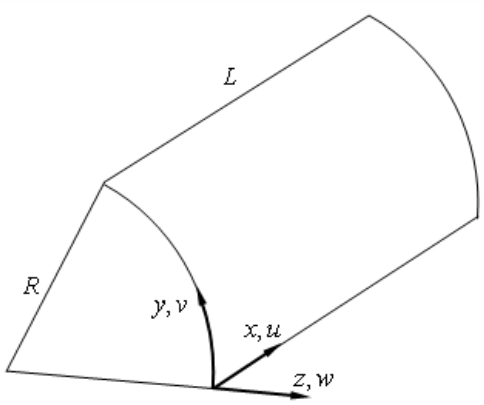

Figure 1. Coordinate system and displacements.

$$\begin{Bmatrix} \varepsilon_x^0 \\ \varepsilon_y^0 \\ \gamma_{xy}^0 \\ \varepsilon_x^1 \\ \varepsilon_y^1 \\ \gamma_{xy}^1 \end{Bmatrix} = \begin{Bmatrix} \dfrac{\partial u_0}{\partial x} \\ \dfrac{\partial v_0}{\partial y} + \dfrac{w_0}{R} \\ \dfrac{\partial v_0}{\partial x} + \dfrac{\partial u_0}{\partial y} \\ -\dfrac{\partial^2 w_0}{\partial x^2} \\ -\dfrac{\partial^2 w_0}{\partial y^2} \\ -2\dfrac{\partial^2 w_0}{\partial x \partial y} \end{Bmatrix} \tag{2}$$

The strains are given by

$$\begin{Bmatrix} \varepsilon_x \\ \varepsilon_y \\ \gamma_{xy} \end{Bmatrix} = \begin{Bmatrix} \varepsilon_x^0 \\ \varepsilon_y^0 \\ \gamma_{xy}^0 \end{Bmatrix} + z \begin{Bmatrix} \varepsilon_x^1 \\ \varepsilon_y^1 \\ \gamma_{xy}^1 \end{Bmatrix} \tag{3}$$

2.2 Constitutive Relations

The linear constitutive relations as per CLST can be expressed as

$$\begin{Bmatrix} \mathbf{N} \\ \mathbf{M} \end{Bmatrix} = \begin{bmatrix} \mathbf{A} & \mathbf{B} \\ \mathbf{B} & \mathbf{D} \end{bmatrix} \begin{Bmatrix} \boldsymbol{\varepsilon}^0 \\ \boldsymbol{\varepsilon}^1 \end{Bmatrix} \text{ or, } \begin{Bmatrix} \boldsymbol{\varepsilon}^0 \\ \boldsymbol{\varepsilon}^1 \end{Bmatrix} = \begin{bmatrix} \mathbf{A}^* & \mathbf{B}^* \\ \mathbf{B}^{*T} & \mathbf{D}^* \end{bmatrix} \begin{Bmatrix} \mathbf{N} \\ \mathbf{M} \end{Bmatrix} \tag{4}$$

The vectors and matrices in Eqn (4) are defined as

$$\mathbf{N} = \begin{Bmatrix} N_x \\ N_y \\ N_{xy} \end{Bmatrix}, \quad \mathbf{M} = \begin{Bmatrix} M_x \\ M_y \\ M_{xy} \end{Bmatrix}$$

$$A_{ij} = \sum_{k=1}^{n} \bar{Q}_{ij}^k (h_k - h_{k+1}) \qquad i, j = 1,2,3$$

$$B_{ij} = \frac{1}{2} \sum_{k=1}^{n} \bar{Q}_{ij}^k (h_k^{\,2} - h_{k+1}^{\,2}) \qquad i, j = 1,2,3$$

$$D_{ij} = \frac{1}{3} \sum_{k=1}^{n} \bar{Q}_{ij}^k (h_k^{\,3} - h_{k+1}^{\,3}) \qquad i, j = 1,2,3$$

$$\{\boldsymbol{\varepsilon}^0\} = \begin{Bmatrix} \varepsilon_x^0 \\ \varepsilon_y^0 \\ \gamma_{xy}^0 \end{Bmatrix}, \quad \{\boldsymbol{\varepsilon}^1\} = \begin{Bmatrix} \varepsilon_x^1 \\ \varepsilon_y^1 \\ \gamma_{xy}^1 \end{Bmatrix} \tag{5}$$

2.3 Energy Formulations

The total potential energy of the grid stiffened composite shell is given by the sum of the strain energy and work done by external forces as

$$\Pi = U + V \tag{6}$$

Strain energy is given by

$$U = \frac{1}{2} \iiint \left(\sigma_x \varepsilon_x + \sigma_y \varepsilon_y + \sigma_z \varepsilon_z + \tau_{xy} \gamma_{xy} + \tau_{yz} \gamma_{yz} + \tau_{xz} \gamma_{xz} \right) dz dx dy \tag{7}$$

In CLST, transverse shear strains are zero and one obtains the following:

$$U = \frac{1}{2} \iint \left(N_x \varepsilon_x^0 + N_y \varepsilon_y^0 + N_{xy} \gamma_{xy}^0 + M_x \varepsilon_x^1 + M_y \varepsilon_y^1 + M_{xy} \varepsilon_{xy}^1 \right) dx dy \tag{8}$$

Then, using Eqn (4), mid-plane strain and mid-plane curvatures (changes) are replaced with compliance matrix elements and force and moment resultants, and one gets the following:

$$\begin{aligned} U = \frac{\Delta}{2} [\; & \left(A_{11}^* N_x^2 + A_{22}^* N_y^2 + A_{66}^* N_{xy}^2 \right) \\ & + 2 \left(A_{12}^* N_x N_y + A_{16}^* N_x N_{xy} + A_{26}^* N_y N_{xy} \right) \\ & + 2 \left(B_{11}^* N_x M_x + B_{22}^* N_y M_y + B_{66}^* N_{xy} M_{xy} \right) \\ & + 2 \left(B_{12}^* N_x M_y + B_{21}^* N_y M_x + B_{16}^* N_x M_{xy} \right) \\ & + 2 \left(B_{61}^* N_{xy} M_x + B_{26}^* N_y M_{xy} + B_{62}^* N_{xy} M_y \right) \\ & + \left(D_{11}^* M_x^2 + D_{22}^* M_y^2 + D_{66}^* M_{xy}^2 \right) \\ & + 2 \left(D_{12}^* M_x M_y + D_{16}^* M_x M_{xy} + D_{26}^* M_y M_{xy} \right) \;] \end{aligned} \tag{9}$$

A convenient way to express the strain energy for Ritz buckling analysis is in terms of the generalised strain vector and stiffness matrix as:

$$U = \frac{1}{2} \int_0^{2\pi R} \int_0^{L} \begin{Bmatrix} \boldsymbol{\varepsilon}^0 \\ \boldsymbol{\varepsilon}^1 \end{Bmatrix}^T \begin{bmatrix} \mathbf{A} & \mathbf{B} \\ \mathbf{B} & \mathbf{D} \end{bmatrix} \begin{Bmatrix} \boldsymbol{\varepsilon}^0 \\ \boldsymbol{\varepsilon}^1 \end{Bmatrix} dx dy \tag{10}$$

The work done by in-plane loads[15] are given by

$$V = \frac{1}{2} \int_0^{2\pi R} \int_0^{L} [\; N_x \left(\frac{\partial w}{\partial x} \right)^2 + N_y \left(\frac{\partial w}{\partial y} \right)^2 + 2 N_{xy} \left(\frac{\partial w}{\partial x} \frac{\partial w}{\partial y} \right) \;] dx dy \tag{11}$$

2.4 Smeared Stiffener Model

A representative unit cell is considered such that by repeating the unit cell the complete system of stiffening ribs can be obtained. (Fig. 2.)

An equivalent shell represented by its length, radius, and the orthotropic stiffness/compliance matrices is considered for buckling analysis. The shell is simply supported at

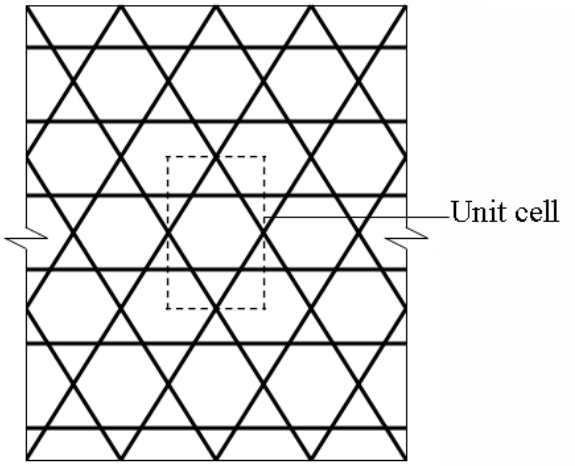

Figure 2. Hexagonal pattern–helical and circumferential ribs.

the bottom-end and free at the top-end. While the length and radius of the equivalent shell are readily obtained from the geometry of the lattice cylinder, the orthotropic stiffness/compliance matrices are obtained by considering strain energy. In line with Eqn (9), under the combined action of the in-plane loads the strain energy of the equivalent shell is given by:

$$U_{equ}=\frac{\Delta_{equ}}{2}\begin{bmatrix}\left(A^*_{11equ}N^2_{xequ}+A^*_{22equ}N^2_{yequ}+A^*_{66equ}N^2_{xyequ}\right)\\+2\left(A^*_{12equ}N_{xequ}N_{yequ}+A^*_{16equ}N_{xequ}N_{xyequ}+A^*_{26equ}N_{yequ}N_{xyequ}\right)\\+2\left(B^*_{11equ}N_{xequ}M_{xequ}+B^*_{22equ}N_{yequ}M_{yequ}+B^*_{66equ}N_{xyequ}M_{xyequ}\right)\\+2\left(B^*_{12equ}N_{xequ}M_{yequ}+B^*_{21equ}N_{yequ}M_{xequ}+B^*_{16equ}N_{xequ}M_{xyequ}\right)\\+2\left(B^*_{61equ}N_{xyequ}M_{xequ}+B^*_{26equ}N_{yequ}M_{xyequ}+B^*_{62equ}N_{xyequ}M_{yequ}\right)\\+\left(D^*_{11equ}M^2_{xequ}+D^*_{22equ}M^2_{yequ}+D^*_{66equ}M^2_{xyequ}\right)\\+2\left(D^*_{12equ}M_{xequ}M_{yequ}+D^*_{16equ}M_{xequ}M_{xyequ}+D^*_{26equ}M_{yequ}M_{xyequ}\right)\end{bmatrix} \quad (12)$$

Surface area of the shell in Eqn (12) is given by $\Delta_{equ}=2\pi R_{equ}L_{equ}$ whereas the force resultants and moment resultants are defined in a conventional way and these correspond to certain load cases stated in Table 1. Using Eqn (12) and Table 1, strain energy expressions for the equivalent cylindrical shell under different load cases are readily obtained. (Each of these expressions has only one unknown compliance matrix element and the corresponding applied load).

The load cases considered in the strain energy formulations of the equivalent shell are also considered in the strain energy formulations of the stiffening ribs. In each load case, the load applied on the equivalent shell is also applied on the lattice cylinder. The load is discretely distributed in the ribs and a simplified force/moment distribution in the unit cell is found out.

Thus, the stress resultants in the rib segments and crossovers in the unit cell are expressed in terms of the applied load and other geometrical parameters describing the lattice members. Different material properties are used for the crossover zones and the ribs and, individual stiffness/ compliance matrix elements for the ribs and crossover zones are found[#]. The compliance matrix elements along with the applied load and the geometrical parameters are utilized to obtain the strain energy expressions of the lattice cylinder under each load case. Total strain energy is obtained by adding the strain energies of the rib segments, helical-to-helical crossovers and helical-to-axial cross overs. Final strain energy expressions are given in *Appendix* 1. Strain energy of the equivalent shell under each load case is equated to that of the lattice cylinder and the corresponding unknown compliance matrix element of the equivalent shell is obtained. (Matrix **B** and A^*_{16equ}, A^*_{26equ}, D^*_{16equ} and D^*_{26equ} are assumed to be zero.)

Table 1. Load cases

Load Case	Non-zero force/moment resultants	Simulated by
1	N_{xequ}	An axial compressive force P_x distributed on the mid-plane.
2	M_{xequ}	An axial compressive force and an axial tensile force, each of magnitude P_x distributed eccentrically by $e/2$ and $-e/2$ respectively wrt the mid-plane.
3	N_{yequ}	A lateral compressive force P_y (by an external pressure p) distributed on the mid-plane.
4	M_{yequ}	A lateral compressive force (by an external pressure p) and a lateral tensile force (by an internal pressure p), each of magnitude P_y distributed eccentrically by $e/2$ and $-e/2$ respectively wrt the mid-plane (Fig. 3.).
5	N_{xyequ}	A torque T_x (by circumferential force distributed on the mid-plane at the top).
6	M_{xyequ}	A torque T_x (by circumferential force distributed eccentrically by $e/2$ wrt the mid-plane at the top) and a torque of the equal magnitude but in opposite direction (by circumferential force distributed eccentrically by $-e/2$ wrt the mid-plane at the top) (Fig. 3.).
7	N_{xequ} and N_{yequ}	Forces described in *Case 1* and *Case 3* applied simultaneously.
8	M_{xequ} and M_{yequ}	Forces described in *Case 2* and *Case 4* applied simultaneously.

[#] Material properties and ply details are indicated in the section on rib unidirectional composites.

3. BUCKLING ANALYSIS

Ritz buckling analysis procedure of minimisation of total potential energy is adopted to determine the critical buckling load of the equivalent composite shell. The generalised displacements are expressed as kinematically admissible expressions for simply supported boundary conditions[2] as follows:

$$u = \sum_{m=1}^{\infty}\sum_{n=1}^{\infty} U_{mn} \cos\alpha x \cos\beta y$$
$$v = \sum_{m=1}^{\infty}\sum_{n=1}^{\infty} V_{mn} \sin\alpha x \sin\beta y \qquad (13)$$
$$w = \sum_{m=1}^{\infty}\sum_{n=1}^{\infty} W_{mn} \sin\alpha x \cos\beta y$$

where, $\alpha = \frac{m\pi}{L}$ and $\beta = \frac{n}{R}$

Strain-displacement relations as per CLST are used in the energy expressions given in Eqns (10) & (11) and the expression for total energy of the shell is obtained by integration. First derivatives of Π wrt U_{mn}, V_{mn} and W_{mn} are found. For equilibrium, the total potential energy has to be minimum for which the above derivatives are equated to zero and an Eigen value problem is formed. For different values of α and β different applied loads satisfy the equilibrium equations out of which the minimum load is the critical buckling load.

4. FINITE ELEMENT VALIDATION

With a view to check the validity of the smeared stiffener model, finite element modelling of lattice cylinder of hexagonal lattice pattern with helical and circumferential ribs was carried out. ANSYS finite element software was used for modelling as well as obtaining a solution. Twenty nodded 3-D layered solid elements were used to model the stiffening ribs (Fig. 4). The number of elements used across the width and depth of any stiffener is 1 whereas along the length of the rib segments, different numbers of elements were used in different models depending upon the length of the rib segment. Different real constant tables are used to represent the rib segments, helical-to-helical crossovers and helical-to-circumferential crossovers both in terms of material properties as well as ply construction.

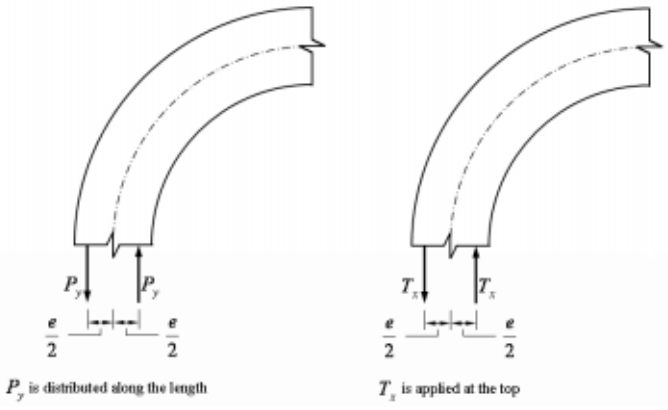

Figure 3. Simulation of M_{yequ} and M_{yequ}.

Several representative cases (Table 2) covering broad and practical ranges of different parameters, viz., radius, $\frac{L}{D}$ ratio, number of helical ribs and height of ribs, have been considered.

A comparison of smeared stiffener model results with finite element results has been made and typical results are given in Table 3 and Fig. 5. Smeared stiffener models, in general, are known to estimate buckling load on the higher side and the present model tends to make estimates in a similar way for low rib thicknesses. For higher rib thicknesses, modelling with single element across rib thickness makes the finite element models too stiff and finite element estimates are found to be on the higher side than found in the estimates of smeared stiffener modelling. Deviation (calculated as percentage of the higher estimate) is the maximum at low rib thickness. Deviations are attributed to the fact that while in the finite element analysis, the ribs are modelled and represented nearly accurately as 3-D discrete structural parts, in the smeared stiffener modelling, the stiffening ribs are converted into an equivalent cylindrical shell based on certain simplistic criteria.

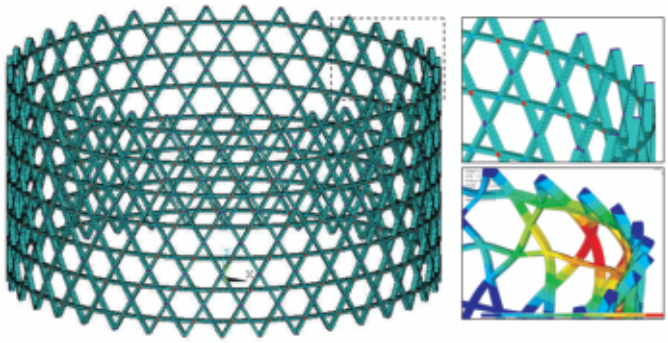

Figure 4. Typical finite element model.

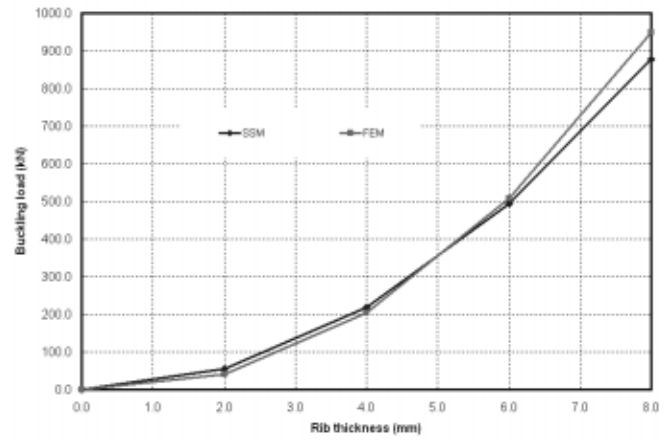

Figure 5. Typical comparison of SSM results with FEM results. Radius of shell=500 mm; No. of helical pair of ribs=45; L/D=0.73; width of ribs=4 mm.

Table 2. Lattice models for finite element modelling

Radius, R (mm)	$\frac{L}{D}$ ratio	No. of helical rib pairs, N_h	Width of ribs, *b* (mm)	Rib thickness, *h* (mm)	No. of models
250	0.53, 0.76, 0.98	36, 45	3, 4, 5	0.5b, b, 1.5b, 2b	72
500	0.48, 0.73, 0.97	45, 60	4, 6, 8	0.5b, b, 1.5b, 2b	72
750	0.48, 0.73, 0.98	45, 60	6, 8, 10	0.5b, b, 1.5b, 2b	72
1000	0.45, 0.73, 1.00	60, 72	8, 10, 12	0.5b, b, 1.5b, 2b	72

Table 3. Comparison of typical SSM results with FEM results.

L/D	h/b	Buckling load (kN)		Deviation (%)
		SSM	FEM	
0.48	0.5	54.4	40.8	25.0
	1.0	220.2	206.3	6.3
	1.5	494.2	516.9	4.4
	2.0	877.4	963.1	8.9
0.73	0.5	54.4	40.5	25.6
	1.0	218.2	203.9	6.6
	1.5	494.2	508.4	2.8
	2.0	877.4	948.9	7.5
0.98	0.5	54.4	40.4	25.7
	1.0	218.9	203.1	7.2
	1.5	494.2	506.0	2.3
	2.0	877.4	942.6	6.9

Radius of shell=500 mm; No. of helical pair of ribs=45; Width of ribs=4 mm

5. RIB MATERIAL *VERSUS* UD COMPOSITE

The ribs in a composite lattice cylindrical shell are essentially unidirectional in character; but their strength and stiffness properties are affected by the presence of the cross-over zones. Fibre volume fraction of rib unidirectional composites can be as low as 50 per cent of that of normal unidirectional composites. (In a lattice cylinder, the crossover zones would correspond to normal unidirectional composites at either $[+\theta/-\theta]$ or $[+\theta/90]$ or $[-\theta/90]$ and the rib segments would correspond to rib unidirectional composites at either $[+\theta]$ or $[-\theta]$ or $[90]$.) Experimental studies carried out elsewhere on specially designed specimens show that rib unidirectional composite properties are distinctly different from (lower than) normal unidirectional composite properties. In this study, material properties for carbon/epoxy system have been taken as follows:

Rib unidirectional composite:

E_1 = 108GPa, E_2 = 8.0GPa, G_{12} = 4.8GPa, and ν_{12} = 0.21.

Normal unidirectional composites:

E_1 = 180GPa, E_2 = 10.0GPa, G_{12} = 6.0GPa and ν_{12} = 0.28.

6. CONCLUSION

An energy-based smeared stiffener model has been developed for global buckling analysis of a composite lattice cylindrical shell of hexagonal lattice pattern formed by filament wound helical and circumferential ribs. Ritz energy-based approach is adopted in the buckling analysis. The smeared stiffener model developed along with Ritz buckling analysis approach is found to be much faster than finite element modelling, thus it facilitates trying out several combinations of design parameters, within the scope of above said lattice pattern, in an efficient way, and thereby, the designer can come to an optimal configuration. The rib segments and the crossovers are duly represented in terms of material properties and ply construction in the strain energy formulation, and thus in this model, difference in rib material structure from crossover material structure is accounted for. Extensive finite element modelling covering different representative sizes have been carried out and, given the intended usage of the model, good comparison between finite element results and results of smeared stiffener modelling has been obtained.

REFERENCES

1. Vasiliev, V.V.; Barynin, V.A. & Rasin, A.F., Anisogrid lattice structures–survey of development and application. *Composite Structures*, 2001, **54**, 361-70.
2. Jones, R.M. Buckling of circular cylindrical shells with multiple orthotropic layers and eccentric stiffeners,

AIAA Journal, 1968, **6**(12), 2301-305.
3. Velmurugan, R. & Buragohain, M. Buckling analysis of grid-stiffened composite cylindrical shell. *J. Aero. Sci. Technol.*, 2007, **59**(4), 282-93.
4. Wodesenbet, E.; Kidane, S. & Pang, S. Optimisation for buckling loads of grid-stiffened composite panels, Composite Structures, 2003, **60**, pp. 159-69.
5. Kidane, S.; Li, G.; Helms, J.; Pang, S. & Woldesenbet, E., Buckling load analysis of grid-stiffened composite cylinders. *Composites Part B: Engineering*, 2003, **34**, 1-9.
6. Jaunky, N.; Knight, N.F. & Damodar, R.A., Formulation of an improved smeared stiffener theory for buckling analysis of grid-stiffened composite panels, *Composites Part B: Engineering*, 1996, **27B**, 519-26.
7. Jaunky, N. & Knight, N.F. Optimal design of grid-stiffened composite panels using global and local buckling analyses. *Journal of Aircraft*, 1998, **35**, 478-86.
8. Damodar, R.A. & Jaunky, N. Optimal design of grid-stiffened panels and shells with variable curvature. *Composite Structures*, 2001, **52**, 173-80.
9. Slinchenko, D. & Verijenko, V.E. Structural analysis of composite lattice shells of revolution on the basis of smearing stiffness. *Composite Structures*, 2001, **54**, pp. 341-48.
10. Huybrechts, S. & Tsai, S.W. Analysis and behaviour of grid structures. *Compo. Sci. Technol.*, 1996, **56**, 1001-015.
11. Wang, J.T.S., Discrete analysis of stiffened composite cylindrical shells. *AIAA Journal*, 1985, **23**(11), 1753-760.
12. Jaunky, N. & Knight, N.F. An assessment of shell theories for buckling of circular cylindrical laminated composite panels loaded in axial compression, *Int. J. Solids Struct.*, 1998, **36**, pp. 3799-820.
13. Geier, B. & Singh, G., Some simple solutions for buckling loads of thin and moderately thick cylindrical shells and panels made of laminated composite material, Aeros. Sci. Technol., 1997, **1**, 47-63, .
14. Reddy, J.N. Mechanics of laminated composite plates and shells. CRC Press.
15. Timoshenko, S.P. & Gere, J.M. Theory of elastic stability. McGraw-Hill Book Co.

Contributors

Dr R. Velmurugan is presently Associate Professor at the Composites Technology Centre, Department of Aerospace Engineering, IIT Madras, Chennai. He has about 15 years of teaching and research experience. He has guided more than 30 students for Masters and Doctoral degree programme. His areas of research include: Impact mechanics, composite analysis and structural crashworthiness.

Mr Manoj Kumar Buragohain obtained his BSc(Engg) from REC, Rourkela in 1990, MTech from IIT Madras in 1992, and PGDFA(CFA) from ICFAI Hyderabad, in 2000. He is currently pursuing PhD from IIT Madras. He has worked for design and development of composite products for structural and ablative applications. He has developed products using filament winding, tape winding, rosette lay-up and contact lay-up. He has developed filament winding programmes for geodesic and non-geodesic helical paths on axisymmetric as well as non-axisymmetric components. His ares of interest include: pressure vessel, composite motor casing, grid-stiffened shell and panel, etc.

Appendix 1

Strain Energy Formulations–Helical and Circumferential Ribs

$$U_{P_x rib} = \frac{LA^*_{11rib}P_x^2}{4\pi Rb\cos^3\theta}\left[\frac{\pi R}{N_h}\left(1+\sin^3\theta\right)-\frac{b}{2\cos\theta}\left(1+2\sin\theta+2\sin^3\theta\right)\right] \tag{A1}$$

$$U_{P_x hco} = \frac{LP_x^2}{4\pi R\cos^4\theta}\left(A^*_{11hco}\cos^4\theta + A^*_{22hco}\sin^4\theta\right) \tag{A2}$$

$$U_{P_x cco} = \frac{LP_x^2A^*_{11cco}\sin\theta}{4\pi R} \tag{A3}$$

$$U_{eP_x rib} = \frac{LD^*_{11rib}e^2P_x^2}{4\pi Rb\cos^3\theta}\left[\frac{\pi R}{N_h}\left(1+\sin^3\theta\right)-\frac{b}{2\cos\theta}\left(1+2\sin\theta+2\sin^3\theta\right)\right] \tag{A4}$$

$$U_{eP_x hco} = \frac{Le^2P_x^2}{4\pi R\cos^4\theta}\left(D^*_{11hco}\cos^4\theta + D^*_{22hco}\sin^4\theta\right) \tag{A5}$$

$$U_{eP_x cco} = \frac{Le^2P_x^2D^*_{11cco}\sin\theta}{4\pi R} \tag{A6}$$

$$U_{P_y rib} = \frac{P_y^2A^*_{11rib}}{384N_hL\pi Rb\sin^4\theta\cos^2\theta}\begin{bmatrix}8\pi^3R^3\cos^3\theta\left(7+19\sin^3\theta\right)\\-12\pi^2R^2N_hb\cos^2\theta\left(1+8\sin\theta+8\sin^3\theta\right)\\-6\pi RN_h^2b^2\cos\theta\left(1-8\sin^2\theta+8\sin^3\theta\right)\\-N_h^3b^3\left(1+16\sin^3\theta\right)\end{bmatrix} \tag{A7}$$

$$U_{P_y hco} = \frac{P_y^2\pi R}{16L\sin^4\theta}\left(A^*_{11hco}\cos^4\theta + A^*_{22hco}\sin^4\theta\right) \tag{A8}$$

$$U_{P_y cco} = \frac{P_y{}^2\pi R}{4L\sin^3\theta}\left(A^*_{11cco}\cos^4\theta + 4A^*_{22cco}\sin^2\theta\right) \tag{A9}$$

$$U_{eP_y rib} = \frac{e^2P_y^2D^*_{11rib}}{384N_hL\pi Rb\sin^4\theta\cos^2\theta}\begin{bmatrix}8\pi^3R^3\cos^3\theta\left(7+19\sin^3\theta\right)\\-12\pi^2R^2N_hb\cos^2\theta\left(1+8\sin\theta+8\sin^3\theta\right)\\-6\pi RN_h^2b^2\cos\theta\left(1-8\sin^2\theta+8\sin^3\theta\right)\\-N_h^3b^3\left(1+16\sin^3\theta\right)\end{bmatrix} \tag{A10}$$

$$U_{eP_y hco} = \frac{e^2P_y^2\pi R}{16L\sin^4\theta}\left(D^*_{11hco}\cos^4\theta + D^*_{22hco}\sin^4\theta\right) \tag{A11}$$

$$U_{eP_y cco} = \frac{e^2P_y{}^2\pi R}{4L\sin^3\theta}\left(D^*_{11cco}\cos^4\theta + 4D^*_{22cco}\sin^2\theta\right) \tag{A12}$$

$$U_{T_x rib} = \frac{LA^*_{11rib}T_x^2}{2\pi R^3b\sin 2\theta}\left\{\frac{\pi R}{N_h\sin\theta}-\frac{b}{\cos\theta}-\frac{b}{\sin 2\theta}\right\} \tag{A13}$$

$$U_{T_x hco} = \frac{Le^2T_x^2}{4\pi R^3\sin^3\theta\cos\theta}\left(A^*_{11hco}\cos^4\theta + A^*_{22hco}\sin^4\theta\right) \tag{A14}$$

$$U_{T_x cco} = \frac{LT_x^2}{4\pi R^3\cos^2\theta\sin\theta}\left(A^*_{11cco}\cos^4\theta + A^*_{22cco}\sin^2\theta\right) \tag{A15}$$

$$U_{eT_x rib} = \frac{LD^*_{11rib} e^2 T_x^2}{2\pi R^3 b \sin 2\theta}\left\{\frac{\pi R}{N_h \sin\theta} - \frac{b}{\cos\theta} - \frac{b}{\sin 2\theta}\right\} \tag{A16}$$

$$U_{eT_x hco} = \frac{Le^2 T_x^2}{4\pi R^3 \sin^3\theta\cos\theta}\left(D^*_{11hco}\cos^4\theta + D^*_{22hco}\sin^4\theta\right) \tag{A17}$$

$$U_{eT_x cco} = \frac{Le^2 T_x^2}{4\pi R^3 \cos^2\theta\sin\theta}\left(D^*_{11cco}\cos^4\theta + D^*_{22cco}\sin^2\theta\right) \tag{A18}$$

$$U_{P_x P_y rib} = \frac{N_h^2 LbA^*_{11rib}\tan\theta}{\pi R}\left[\begin{array}{l}
\dfrac{P_y^2}{48L^2b^2\tan^2\theta}\left\{\left(\dfrac{\pi R}{N_h\sin\theta} - \dfrac{b}{\sin 2\theta}\right)^3 - \dfrac{2b^3}{\cos^3\theta} + \dfrac{\pi^3 R^3}{N_h^3}\right\} \\
-\dfrac{P_y}{8N_h Lb^2\sin^3\theta}\left(P_x + \dfrac{\pi RP_y}{L\tan^2\theta}\right)\left\{\left(\dfrac{\pi R}{N_h} - \dfrac{b}{2\cos\theta}\right)^2 - b^2\tan^2\theta\right\} \\
+\dfrac{P_y}{8N_h Lb^2}\left(-P_x + \dfrac{\pi RP_y}{L\tan^2\theta}\right)\left(\dfrac{\pi^2R^2}{N_h^2} - \dfrac{b^2}{\cos^2\theta}\right) \\
+\dfrac{1}{4N_h^2b^2\cos^2\theta}\left(P_x + \dfrac{\pi RP_y}{L\tan^2\theta}\right)^2\left(\dfrac{\pi R}{N_h\sin\theta} - \dfrac{b}{\cos\theta} - \dfrac{b}{\sin 2\theta}\right) \\
+\dfrac{\tan^2\theta}{4N_h^2b^2}\left(-P_x + \dfrac{\pi RP_y}{L\tan^2\theta}\right)^2\left(\dfrac{\pi R}{N_h} - \dfrac{b}{\cos\theta}\right)
\end{array}\right] \tag{A19}$$

$$U_{P_x P_y hco} = \frac{\left(2P_x L\sin^2\theta + \pi RP_y\cos^2\theta\right)^2\left(A^*_{11hco}\cos^4\theta + A^*_{22hco}\sin^4\theta\right)}{16\pi RL\sin^4\theta\cos^4\theta} \tag{A20}$$

$$U_{P_x P_y cco} = \frac{L\tan\theta}{4\pi R\cos\theta}\left[\left(P_x + \frac{\pi RP_y}{L\tan^2\theta}\right)^2 A^*_{11cco}\cos^2\theta + \left(\frac{4\pi^2R^2P_y^2}{L^2\tan^2\theta}\right)A^*_{22cco}\right] \tag{A21}$$

$$U_{eP_x eP_y rib} = \frac{e^2N_h^2 LbD^*_{11rib}\tan\theta}{\pi R}\left[\begin{array}{l}
\dfrac{P_y^2}{48L^2b^2\tan^2\theta}\left\{\left(\dfrac{\pi R}{N_h\sin\theta} - \dfrac{b}{\sin 2\theta}\right)^3 - \dfrac{2b^3}{\cos^3\theta} + \dfrac{\pi^3 R^3}{N_h^3}\right\} \\
-\dfrac{P_y}{8N_h Lb^2\sin^3\theta}\left(P_x + \dfrac{\pi RP_y}{L\tan^2\theta}\right)\left\{\left(\dfrac{\pi R}{N_h} - \dfrac{b}{2\cos\theta}\right)^2 - b^2\tan^2\theta\right\} \\
+\dfrac{P_y}{8N_h Lb^2}\left(-P_x + \dfrac{\pi RP_y}{L\tan^2\theta}\right)\left(\dfrac{\pi^2R^2}{N_h^2} - \dfrac{b^2}{\cos^2\theta}\right) \\
+\dfrac{1}{4N_h^2b^2\cos^2\theta}\left(P_x + \dfrac{\pi RP_y}{L\tan^2\theta}\right)^2\left(\dfrac{\pi R}{N_h\sin\theta} - \dfrac{b}{\cos\theta} - \dfrac{b}{\sin 2\theta}\right) \\
+\dfrac{\tan^2\theta}{4N_h^2b^2}\left(-P_x + \dfrac{\pi RP_y}{L\tan^2\theta}\right)^2\left(\dfrac{\pi R}{N_h} - \dfrac{b}{\cos\theta}\right)
\end{array}\right] \tag{A22}$$

$$U_{eP_x eP_y hco} = \frac{e^2\left(2P_x L\sin^2\theta + \pi RP_y\cos^2\theta\right)^2\left(D^*_{11hco}\cos^4\theta + D^*_{22hco}\sin^4\theta\right)}{16\pi RL\sin^4\theta\cos^4\theta} \tag{A23}$$

$$U_{eP_x eP_y cco} = \frac{e^2L\tan\theta}{4\pi R\cos\theta}\left[\left(P_x + \frac{\pi RP_y}{L\tan^2\theta}\right)^2 D^*_{11cco}\cos^2\theta + \left(\frac{4\pi^2R^2P_y^2}{L^2\tan^2\theta}\right)D^*_{22cco}\right] \tag{A24}$$